

# Performance Analysis of Integrated Nuclear-Solar Energy System Sharing Same Molten Salt Thermal Energy Storage

Soto G J<sup>1</sup>, Wagner M J<sup>2</sup>, Neises T W<sup>3</sup>, Lindley B A<sup>1\*</sup>

<sup>1</sup> Department of Engineering Physics, University of Wisconsin-Madison, 1500 Engineering Drive, Madison, WI 53706, USA

<sup>2</sup> Department of Mechanical Engineering, University of Wisconsin-Madison, 1415 Engineering Drive, Madison, WI 53706, USA

<sup>3</sup> National Renewable Energy Laboratory, Thermal Systems Group, 15013 Denver West Parkway, Golden, CO 80401, USA

\*Corresponding author: [lindley2@wisc.edu](mailto:lindley2@wisc.edu)

## Abstract

Advanced nuclear reactors may be deployed with integrated thermal energy storage to improve flexibility and maximize revenue. This presents opportunities for thermal integration with concentrating solar power (CSP) to generate component synergies and/or improve performance. In this study, a computational model is developed for an integrated nuclear and CSP system that both share the same molten salt thermal energy storage (TES). Optimized dispatch schedules are developed subject to various market conditions, and the ratio of the nuclear to CSP thermal output is also varied. Performance of the combined system is compared to separate nuclear and solar plants, to determine if there is an overall benefit that can be derived from sharing the TES. Given sufficient volatility in electricity prices (e.g., under CAISO market conditions), synergies of up to 8% in net revenue are observed as a result of sharing the same TES, primarily due to improved revenue from enabling operation of the turbine closer to its design point, as well as being able to better take advantage of higher electricity prices. The synergy benefits are largest when the nuclear and solar plants have similar thermal output. However, when prices are less volatile the opposite behavior can be observed and it can be preferable to operate the nuclear plant as a baseload generator.

## 1. Introduction

Nuclear power plants (NPPs) are typically employed as baseload generators due to their low variable costs. However, as energy markets experience increased penetration of variable renewable energy (VRE) sources, the variability in electricity prices increases [1]. Solar energy contributes to the grid during daylight hours; however, the times of maximum demand are in the early morning and late afternoon. The misalignment of solar availability and peak grid demand results in greater fluctuation of wholesale energy prices over the day. Notably, VRE-saturated markets such as the California Independent System Operator market (CAISO) in the western United States witness negative values in prices during the middle of the day. These prices, however, surge rapidly in the evening as residential load intensifies and solar power reduces [2]. This motivates the development of economic load following strategies NPPs [3] [4], [5]. This can be challenging because of their high fixed and low variable costs, which make it difficult for NPPs to be profitable without maximizing the use of the asset.

One possible technology that enables nuclear plants to change power output while continuing to maximize use of the asset is thermal energy storage (TES). Integrated TES allows the nuclear plant to maintain a constant thermal output while reducing electricity production during unfavorable pricing periods by storing some of its thermal energy for later use. Once the electricity prices rises, the NPP can convert the

excess stored heat into electricity. This requires overspecification of the power conversion cycle to accommodate periods of higher electrical generation, which increases capital costs, but then presents opportunities for increased revenue. One considered configuration for nuclear + TES is to use the nuclear reactor to heat molten salt which can be stored in a two-tank system and dispatched when desired. This configuration is inspired by existing concentrating solar power (CSP) plants, which heat up molten salt directly for later dispatch [6].

Such configurations then motivate the study of integration of CSP into the overall nuclear-TES system. Prior work includes many examples of thermal integration of nuclear and solar power where by the advantages of both technologies are combined to achieve more flexible operation and lower-cost power:

- Ref [7] investigated a hybrid system with a light water reactor indirectly heating steam at 255°C, which is subsequently superheated using molten salt from a CSP power tower at 565°C. The molten salt TES is directly linked to the CSP, and the nuclear reactor is indirectly coupled to the TES. Here, optimal economic performance of the combined system was observed when the nuclear and solar plants produced similar electrical outputs. Various TES fluids were compared, and Therminol was selected as being most economic.
- Refs [8] [9] similarly proposed use of a CSP power tower to superheat the output of a nuclear reactor operating at lower temperature, resulting in increased thermodynamic efficiency of the combined plant.
- Ref [10] investigated coupling a nuclear reactor and CSP power tower at similar operating temperatures to a packed bed TES. The optimal system was found to combine similar capacities of CSP and nuclear reactors with 15 hours of thermal energy storage. This was based on an assessment of system efficiency and ability to meet a prescribed load.
- Ref [11] considers integration of parabolic trough CSP into the feedwater heaters of a nuclear reactor with a steam Rankine cycle as a means of boosting efficiency. A transient analysis of a similar system is performed in Ref. [12].

The present study investigates a system in which a nuclear reactor (similar to that considered by multiple nuclear reactor vendors [5], [13], [14]) operates at a temperature compatible with current molten salt TES. The reactor shares TES with a solar power tower. The motivation for such a configuration is to derive cost synergies from sharing the TES, with respect to separate nuclear and CSP plants both with their own TES. The study evaluates several possible synergies, including:

- The ability to co-optimize performance to make best use of the molten salt TES and turbine to maximize revenue by generating when electricity prices are high while keeping the turbine closer to its design point during the times when electricity is being generated.
- Component synergies arising from shared balance of plant equipment for both heat sources.

These synergies must be balanced against the additional complexity of combining the two heat sources, and the requirement of co-siting them, as both nuclear and solar plants have specific siting considerations.

To this end, the design and optimized dispatch of the hybrid plant is analyzed and compared to equivalent separate plants to quantify the potential synergistic benefit. We furthermore investigate how any such gains depend first on the relative size of the nuclear and solar plants and second on the volatility of electricity prices. This fills a gap in the literature by quantifying *whether* such synergy exists, and by providing a rigorous analysis of system performance when both nuclear and CSP can charge the same TES.

This work additionally describes a new capability to perform computational analysis of such systems that derives from the System Advisor Model (SAM), which was developed by National Renewable Energy Laboratory [15]. In our previous work, we adapted SAM to model nuclear-only systems [16] and performed a dispatch optimization of a nuclear reactor integrated with a molten salt TES. It was found that including a TES and correspondingly oversizing the turbine of the reactor could achieve an overall economic benefit in markets with sufficiently volatile electricity prices. Under CAISO market conditions (where electricity prices are lower around midday) with economically optimal plant design, the turbine typically shut down in the middle of the day and operated at or close to the design point at other times. This model is herein further extended to the nuclear-solar hybrid configuration of interest.

From a safety perspective, non-water-cooled reactors (with temperatures compatible with the system presented here) may not need nuclear safety classified systems beyond the primary heat exchanger. The hybrid plant proposed here is most applicable to concepts that achieve this. It is in principle achievable due to a few factors:

- Radioactive release from the core can in principle be limited so that a simplified containment design can be used, that does not need to withstand high pressure and may employ filtered vents. This is used in the Westinghouse LFR [17] and is a common design option for HTRs [18], [19].
- The coupling between secondary and primary is weaker and does not lead to as large a reactivity insertion. Overcooling transients can hence be classified as an anticipated operating occurrence.

The heat exchanger to the working fluid is typically a safety classified system as it presents an opportunity for fission products to be released into the secondary. The safety classification of the steam generators can however vary significantly between advanced reactor types. Low pressure primary coolants (SFRs, LFRs and molten salt-cooled reactors) can help confine fission products to the primary system even in the event of a leak in the heat exchanger. Chemical compatibility issues (e.g., sodium/water) may also play a role, depending on the advanced reactor type and configuration over the primary/secondary/tertiary. It is noted that some SFRs contain safety classified components in the steam generation system (e.g. Ref. [20]), but recent designs such as the Westinghouse LFR [17] and Natrium [21] target eliminating nuclear safety systems from the power island.

Therefore, nuclear safety and licensing cost complexity should not present a significant obstacle to the scheme presented here. In all cases, the additional complexity of the IES should nonetheless be considered in the probabilistic safety analysis, including:

- Failures of any additional components (e.g., heat exchangers, turbines) and
- Failures in heat users or other heat generators (e.g., implications of accident at coupled industrial facility, or coupled solar thermal plant, thermal energy storage).

## **2. Methodology**

### **2.1. Reactor, CSP and Plant Modelling Assumptions**

A nuclear reactor is modelled in series with a CSP system as shown in Figure 1. The power level of the nuclear reactor is varied in this study, with a reference thermal output of 950 MW<sub>th</sub> taken from the Westinghouse LFR [17]. This baseline is selected for consistency with our nuclear-only study [16], and the reference electrical output from that study of 450 MWe is also used to set the design point thermodynamic efficiency of the power cycle. This efficiency is used throughout this study and is higher than typical for a

system using a solar salt. However, the thermodynamic efficiency does not affect the comparison between the results, since the revenue will scale with the thermodynamic efficiency at the design point across all cases.

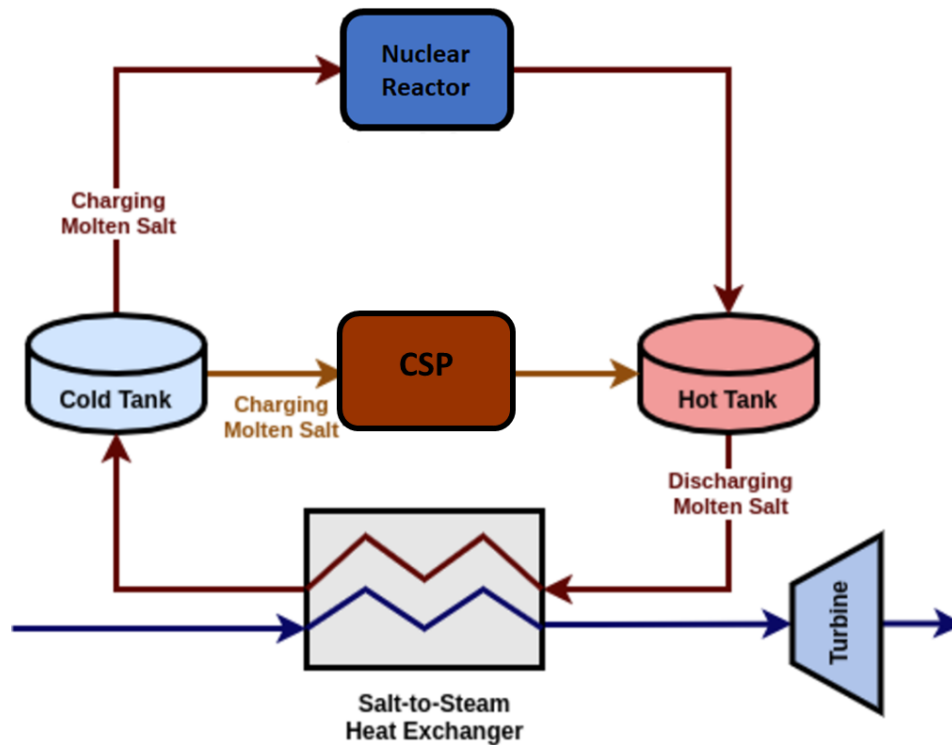


Figure 1: Hybrid Energy System comprising Nuclear, Solar and TES

The economic performance of the integrated energy system is evaluated using SAM financial modules which calculate a minimum viable power purchase agreement (PPA) price for the site, as described in Ref. [16]. A lower PPA indicates that the plant is more competitive. The PPA price represents a minimum commercially viable wholesale price of energy. An internal rate of return of 11% is specified, along with a payback time of 20 years; the PPA is the price at which these conditions can be met. The goal here is not a techno-economic comparison of nuclear and CSP, but instead to evaluate whether synergies can be realized when combining them into a single plant, compared to having separate plants.

A CSP power tower design is specified and generated using SAM and the integrated SolarPILOT layout tool [22]. The design point DNI is  $950 \text{ W/m}^2$  and the receiver thermal power is 670 MWth. The CSP design includes 8790 heliostats totaling  $1.27 \times 10^6 \text{ m}^2$  of mirror area with a pre-generated collector field arrangement and flux map. The receiver is placed at a height of 193m with its height and width of 21.6m and 17.6m respectively. Each TES storage tank is 12 m tall, and 15 tank pairs (hot and cold) equally share the salt inventory. The power tower design is held constant throughout this study to avoid needing to reoptimize the plant design. Instead, the effect of altering the ratio of nuclear to solar thermal generation can be readily examined by adjusting the nuclear output.

To facilitate cross comparison, the weather data is fixed across the three cases to Phoenix, AZ. This is selected as it is an attractive location for a CSP plant due to favorable weather and available land area. A

“typical” year of weather data at this location (formed utilizing aggregated data across several years) is utilized in SAM.

Optimal operating schedules for each subsystem in Figure 1 are first generated using a dispatch model. An engineering model in SAM Simulation Core (SSC) then resolves energy balances for the hybrid plant at each time step. The procedure described in Ref. [16] is adapted to incorporate both nuclear and solar plant models. As in our previous work, pre-generated tabular performance data for the steam Rankine power conversion cycle is utilized to capture on- and off-design performance [23].

### 2.1.1 Reactor, CSP and Plant Thermodynamics in SSC

NREL originally developed a control and solver in SSC to set the operations of the power tower, TES, and power cycle by ensuring feasibility (e.g., obeying maximum mass flow rates) and balance mass and energy while trying to achieve cycle output targets given by the plant dispatch signal. The controller solver determines discrete operating modes for each component and then determines how to allocate mass flow between components to balance mass and energy. From Ref. [16], an SSC module was created for a nuclear reactor core supplying constant thermal power to a power cycle with TES.

For the present work, we added the nuclear reactor as heat source that can heat the salt heat transfer fluid (60% NaNO<sub>3</sub> and 40% KNO<sub>3</sub>) in parallel with the power tower. We model the reactor to supply constant thermal power to the heat transfer fluid. We added the nuclear heat transfer fluid steam to our energy and mass balances, applying an enthalpy mixer with the parallel power tower stream. The addition of the reactor as a parallel heat source also requires adding logic to the controller to accommodate the requirement that the reactor generate its design-point heat output every timestep of the simulation.

SSC required new modules to accommodate two thermal providers to the power conversion cycle – the nuclear reactor and the CSP tower – each with new operating modes for the thermodynamic, energy balance, and mass flow balance solvers. From Ref. [16], an SSC module was created for a nuclear reactor core supplying constant thermal power to a power cycle with TES. SSC also contained a detailed model and solvers for a CSP system supplying variable power to a power cycle with TES. Operating modes exist for the nuclear reactor, TES, power cycle (PC), and CSP components individually as shown in Table 1.

Table 1: Operating modes in SSC for the four components of the Hybrid system.

Power Cycle	Thermal Storage	Nuclear Reactor	CSP
OFF	OFF	ON	OFF
Start-up	Empty		Start-Up
Standby	Charge		To Cold
Min-Power	Discharge		Defocus
RM_LO (near min)	Full		ON
Target			
RM_HI (near max)			
Max-Power			

The main PC operating modes include an ‘off’, ‘start-up’, ‘min-power’, ‘target’ and ‘max-power’ mode. The ‘target’ mode allows user-input for the desired electric power output; for this study, results from a lower fidelity dispatch optimization problem were used. An ‘RM\_LO’ and ‘RM\_HI’ operating mode are also used

where operations are near the minimum and maximum power-rating but require more tolerance. The TES operating modes include an ‘off’, ‘charge’ and ‘discharge’ mode with two additional modes— ‘empty’ and ‘full’—when the energy levels in the hot tank need to be either emptied or filled. The CSP modes include ‘off’, ‘start-up’, ‘to-cold’ (where some flow is routed to the cold tank to maintain proper temperatures and state of the molten salt), ‘defocus’ (where the thermal power to the receiver is throttled), and ‘on’.

Within the nuclear reactor SSC module from Ref. [16], thermodynamic calculations and solvers were applied for combinations of all operating modes of the PC, TES and reactor. A previous SSC module for CSP already existed for receiver power tower, collector field of heliostats and molten salt flow loop from cold to receiver to hot tank; solvers also were in place to resolve thermodynamics of the CSP, PC and TES operating mode combinations. A new “dual” SSC module and solver was added to combine operating modes accounting for both reactor and CSP thermal power. Since two mass flow streams now had to be modeled entering the hot tank and drawn from the cold tank (due to the CSP and reactor operating independently), new calculations for resultant mass flow balance, inlet and outlet temperatures and energy balances needed to be modified. Of note are the following operating modes

- Reactor is **ON** while the CSP is **OFF**
- Reactor and CSP are both **ON**
- Reactor is **ON** while CSP is in **STARTUP**

which cause different outlet temperatures for the molten salt heading into the hot tank. The first case can be modeled as a single mass flow stream from the reactor entering the hot tank in Figure 1. The second case results in slightly different temperatures with at most a 10 degree C difference, where some sort of mixing should be calculated between the two molten salt streams into the hot tank. The third would result in bigger disparities in outlet temperature as the CSP is in start-up mode, therefore proper enthalpy balance must be applied and were implemented here.

## 2.2. Market Structure

Final costs of the CSP model, which are calculated within SSC, include individual cashflows for the heliostat, tower, and receiver. The system costs are taken from the default SAM values [15] and are discussed briefly here. However, the exact values are not particularly important as the goal is to establish a representative baseline cost in order to perform comparative studies. The heliostat costs are \$140/m<sup>2</sup> for an assumed area of 1.27x10<sup>6</sup>m<sup>2</sup> (each of the 8790 heliostats is approximately 12m x 12m). The tower costs are calculated in Eq. (1), where  $K_{tower}$  is \$3M and the scaling factor  $\lambda_{tower}$  is 0.0113.

$$C_{tower} = K_{tower} e^{\lambda_{tower} \left( h_{tower} - \frac{h_{rec}}{2} + \frac{h_{helio}}{2} \right)} \quad (1)$$

Receiver costs are a function of the receiver area as characterized by Eq. (2), where  $K_{rec}$  is \$103M with reference area of 1571 m<sup>2</sup> and scaling factor  $\lambda_{rec}$  of 0.7. For a receiver with dimensions 21m x 17m, the final receiver cost is \$36M.

$$C_{rec} = K_{rec} \left( \frac{A_{rec}}{A_{ref}} \right)^{\lambda_{rec}} \quad (2)$$

A power law model in Eq. (3) computes the turbine cost in order to account for the wide range in power plant sizes and evaluate potential synergy effects from the integrated plant.

$$C_{turbine} = KP^{\lambda_{turbine}} \quad (3)$$

Here,  $P$  is the power of the turbine,  $C$  is the cost of the turbine and  $K$  is a constant set to give \$400/kWe cost at 450 MWe electrical output, consistent with our previous study [16]. The power law exponent is  $\lambda_{turbine} = 0.77$  [24]. The nuclear reactor is assigned a fixed cost of \$3750, not accounting for the balance of plant [16]. It is noted that such ‘economy of scale’ cost curves do not necessarily extrapolate to large plants, as other effects (such as economy of volume) become important. Nonetheless, the effect of turbine cost scaling on this study is quite mild, and relatively easy to separate.

Three tariff schedules shown in Figure 2 are considered:

- A “generic” tariff schedule from SAM that can be used to test responses to both seasonal and daily changes in price profile. Further discussion about use of this profile is provided in our previous paper [16].
- Two time series from CAISO data. These are locational marginal prices (LMP) generated from the online OASIS tool [25]. The LMP are normalized to enable a consistent comparison of revenues between cases. Two sets of CAISO tariff data are used:
  - Palo Verde (PALOVRDE\_5\_N101) node taken 1 Jan to 31 Dec 2022 is selected for consistency with the site location of the solar plant. It is also a plausible location for a nuclear-solar IES, as it is the site of an existing nuclear generating station and in an area of high solar irradiance.
  - Iron Mountain (IRONMTN\_2\_N001) node taken from 1 Jan to 31 Dec 2019 is selected to facilitate cross-comparison with Ref. [16].

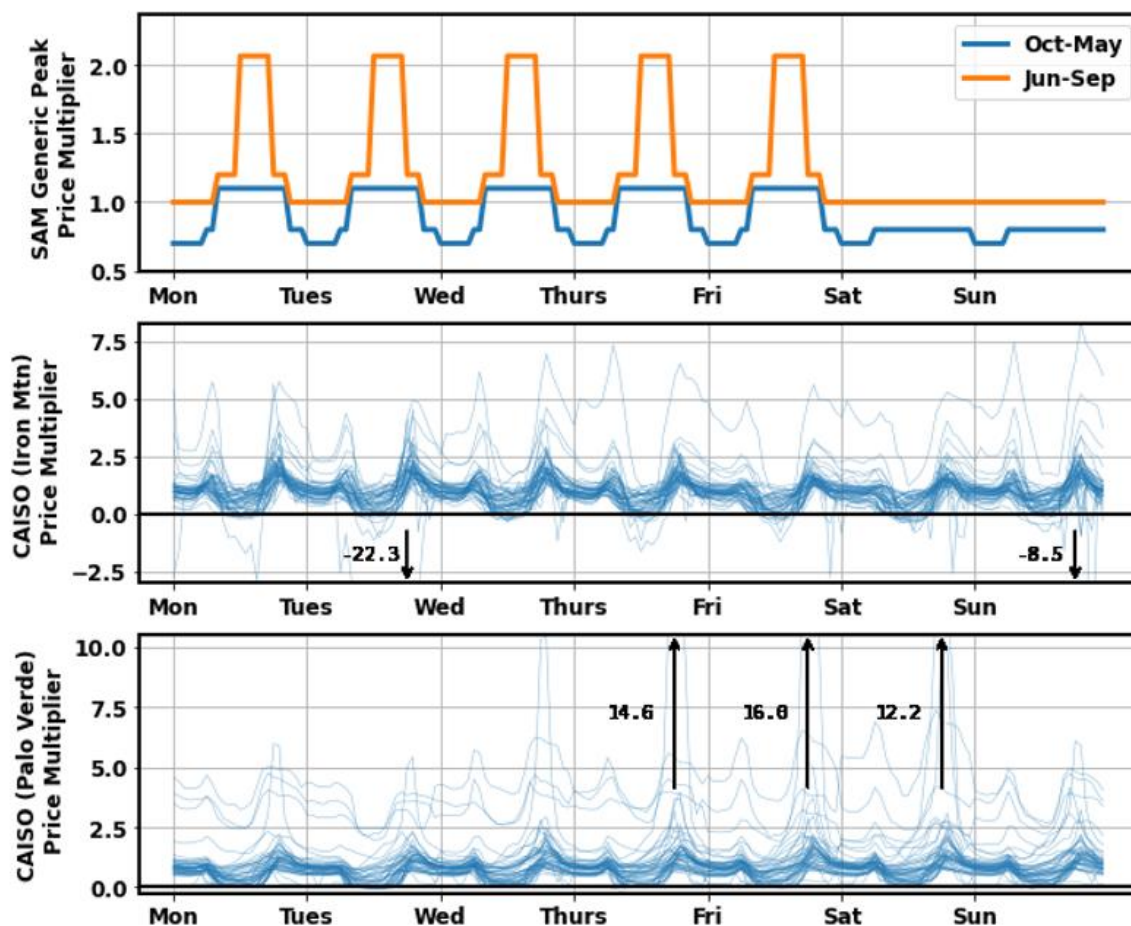


Figure 2: Price multipliers used to simulate different market conditions: (top) generic peak pricing schedule from SAM and (middle and bottom) normalized LMPs from CAISO. Some extreme values are annotated on the graph.

Both the CAISO tariffs exhibit significantly more volatility in prices than the SAM generic tariffs. The Palo Verde 2022 tariffs include little to no negative pricing, whereas the Iron Mountain 2019 tariffs have many instances of negative pricing. In both cases, there is a substantial peak in pricing towards the evening.

CAISO tariffs have been used in this study as they are readily available online and their general daily trends are representative of electricity markets with increasing VRE generation such as those operating in the U.S. southwest, which is a relatively attractive choice for a hybrid nuclear-CSP plant. The CAISO data used here had a standard deviation in electricity prices of 90-100% of the mean price, compared to 30% for the generic tariff. While this measure alone does not capture all of the complexities of price volatility, it can be used to compare other markets. Comparing to data on electricity price markets in Australia, Europe and North America. in Ref. [26] (published in 2018), CAISO is at the higher end of price volatility and the generic tariff towards the lower end. Nonetheless, many markets have similar volatility to CAISO (including the Australian markets and ERCOT), or levels approaching this volatility (e.g. in areas of Europe), and volatility is expected to increase significantly with higher renewables penetration. Also, the hybrid nuclear-CSP plant proposed here is most applicable to areas of high solar resource, including CAISO, ERCOT and Australia – which tend to have higher price volatility.

The focus of this paper is on the cost comparison of the hybrid plant to the separate plant. Cost comparison of CSP and nuclear is not intended here, as only typical costs are used and for nuclear in particular these are aspirational costs for advanced reactors that have not yet been built, rather than actual costs for constructed power plants.

### 2.3. Mathematical Formulation of Dispatch Optimization Problem

We generate optimal energy dispatch schedules for the combined plant using a mixed-integer linear programming (MILP) paradigm developed from Refs. [27], [28] combined with the nuclear-storage model in Ref. [16]. The MILP problem is implemented using Pyomo [29], calculating the initial operating state of the nuclear plant, power cycle, molten salt tank and CSP subsystems. Other parameters include the tariff rate  $P_t$  for each time step of the time horizon  $\mathcal{T}$ . The full variable list can be found in Refs. [16] and [20]. The objective of the combined model is summed overall time steps in the time horizon  $\mathcal{T}$  as shown in Eq. (4).

$$\begin{aligned} \max \sum_{t \in \mathcal{T}} & [\Delta t P_t (\dot{w}_t^s - \dot{w}_t^p) - C^{csu} y_t^{csup} - C^{chsp} y_t^{chsp} - \alpha y_t^{csd} - C^{\Delta w} (\dot{w}_t^{\Delta+} + \dot{w}_t^{\Delta-}) \\ & - C^{vw} (\dot{w}_t^{v+} + \dot{w}_t^{v-}) - C^{rsu} y_t^{rsup} - C^{rhsp} y_t^{rhsp} - \alpha y_t^{rsd} \\ & - \Delta t (C^{pc} \dot{w}_t + C^{csb} Q^b y_t^{csb} + C^{nuc} x_t^n + C^{rec} x_t^r)] \end{aligned} \quad (4)$$

The first term represents the revenue of the plant from variable electricity sales  $\dot{w}_t^s$  (with potential of purchasing some electricity  $\dot{w}_t^p$  if necessary) sold at a given price tariff  $P_t$ . From this revenue term we subtract various costs. The first two negative costs are penalties for “cold” or “hot” power cycle start-up operations, respectively, with associated costs  $C^{csu}$  and  $C^{chsp}$  along with associated binary variables  $y_t^{csup}$  and  $y_t^{chsp}$ . A shutdown cost for the PC is also subtracted using binary variable  $y_t^{csd}$ . The two subsequent terms penalize excessive power cycle ramping  $C^{\Delta w}$  as well as for ramping past the design point  $C^{vw}$ . Extra cost terms specifically for the CSP receiver tower are also added. Two start-up costs for “cold” and “hot” start-up of the receiver are added with binary variables  $y_t^{rsup}$  and  $y_t^{rhsp}$  and costs  $C^{rsu}$ ,  $C^{rhsp}$  respectively. An additional shutdown cost for the CSP with binary variable  $y_t^{rsd}$  is also subtracted. The final term in the objective function introduces costs associated with production by the power cycle  $\dot{w}_t$ , standby power cycle via binary variable  $y_t^{csb}$ , nuclear thermal power production  $x_t^n$  and CSP receiver power production  $x_t^r$ . The purpose of these costs is to disincentivize equipment operation unless conditions are economically favorable. Additional updated constraints are detailed in Appendix A.

As in our previous work [16], a 48-hour time horizon  $\mathcal{T}$  is used in the dispatch model. The model is solved utilizing the Gurobi solver [30]. The first 24 hours of the solution are used to provide target conditions for the SAM model. The interface between the MILP and SAM is further described in Ref. [16], noting that the key modification here compared to previous work is the incorporation of the CSP power tower into the overall framework as described in Section 2.1.

## 3. Results and Discussion

### 3.1. Solar Cases

A solar-only case is first developed to provide a baseline solar plant to compare with the hybrid cases. To ensure consistency between modelled cases, the hybrid model is utilized, but with the nuclear reactor set to an extremely low thermal output. For each tariff schedule, the turbine size and TES capacity are optimized to produce the minimum PPA. Results are given in Table 2. The SAM generic tariff optimizes to

a relatively large turbine and small TES, whereas both CAISO cases optimize to a smaller turbine and larger TES. The difference in behavior is thought to be because the generic tariff has price peaks coinciding with daytime hours whereas with the CAISO tariffs the peak is in the evening, and for some parts of the year, also the morning.

Table 2: Optimized Solar Plant Configurations

Tariff	SAM	Iron Mountain 2019	Palo Verde 2022
Turbine size (MWe)	260	140	140
TES Capacity (hr)	1	16	14
Year 1 PPA price (c/kWh)	7.90	8.41	8.75
Capacity Factor	24.7%	46.6%	48.6%

The electrical power out and TES charge are recorded for each timestep. The population of values for a given hour of the day are consolidated into a violin plot for both metrics, where the thickness of the plot corresponds to the number of observations at a given value. Profiles are divided according to winter & summer and also according to week & weekend days; corresponding to the different tariff schedules in Figure 2. Subplots distinguish between winter and summer tariffs by column, and each column is further subdivided into a row for weekday and another for weekend tariffs. Results are shown for the optimized CSP plant configurations in Figure 3, Figure 4 and Figure 5

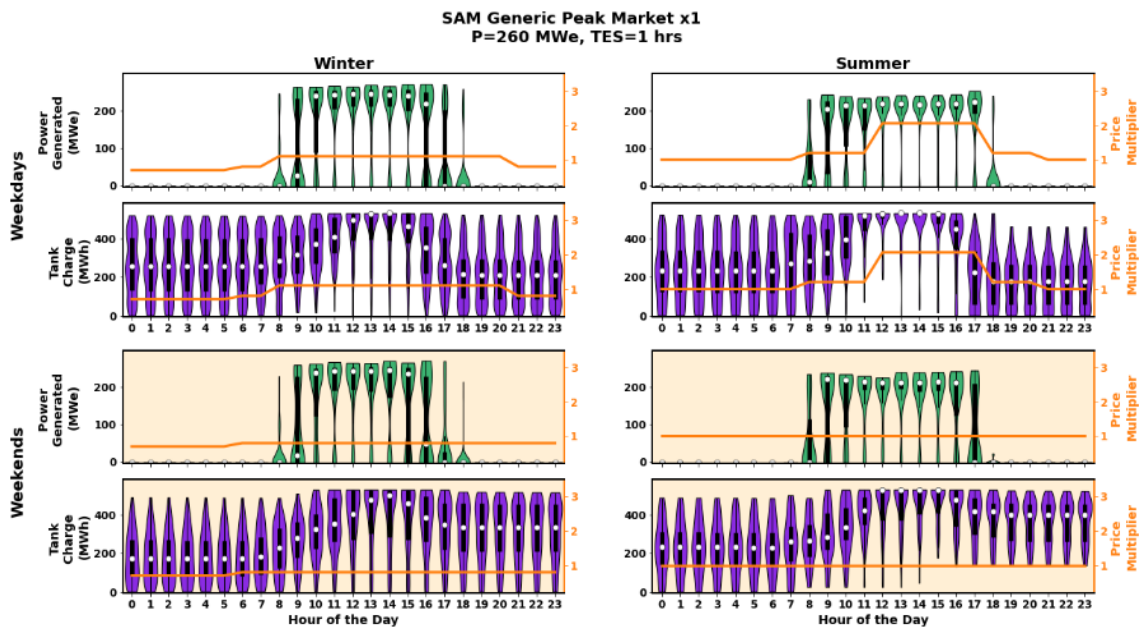


Figure 3: Hourly violin plot distributions for a year of electrical power production for an optimal CSP plant with generic SAM tariff. The white circle is the median value. The black vertical rectangle shows the 25th and 75th percentiles. Price multipliers are displayed on the right axis of each subplot.

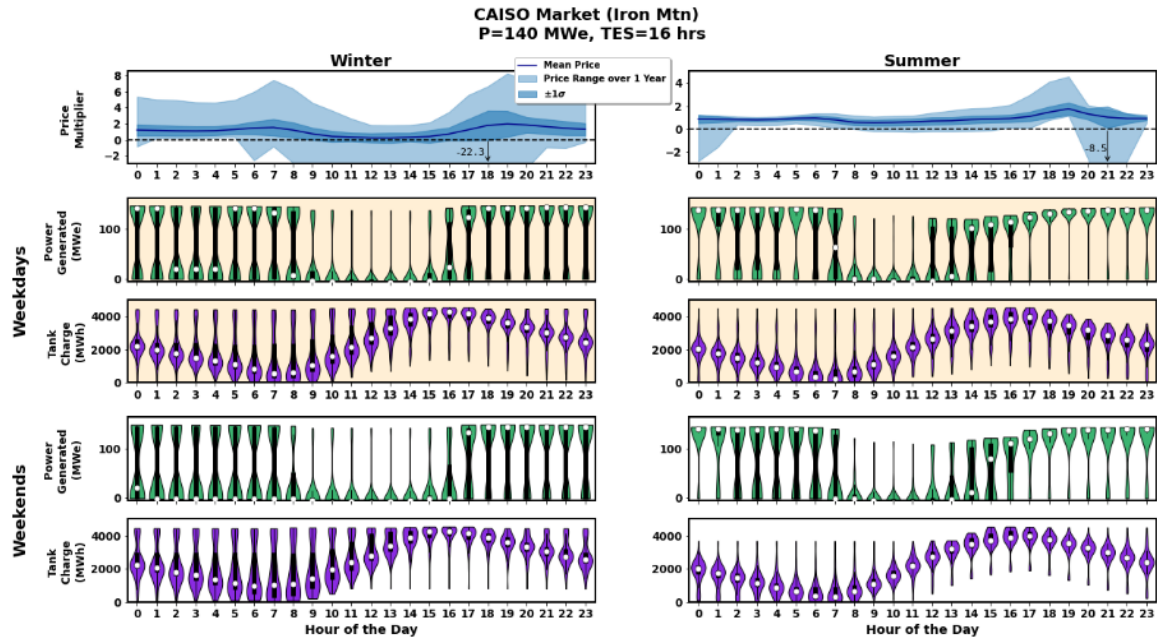


Figure 4: Hourly violin plot distributions for a year of electrical power production for an optimal CSP plant with CAISO tariff (Iron Mountain)

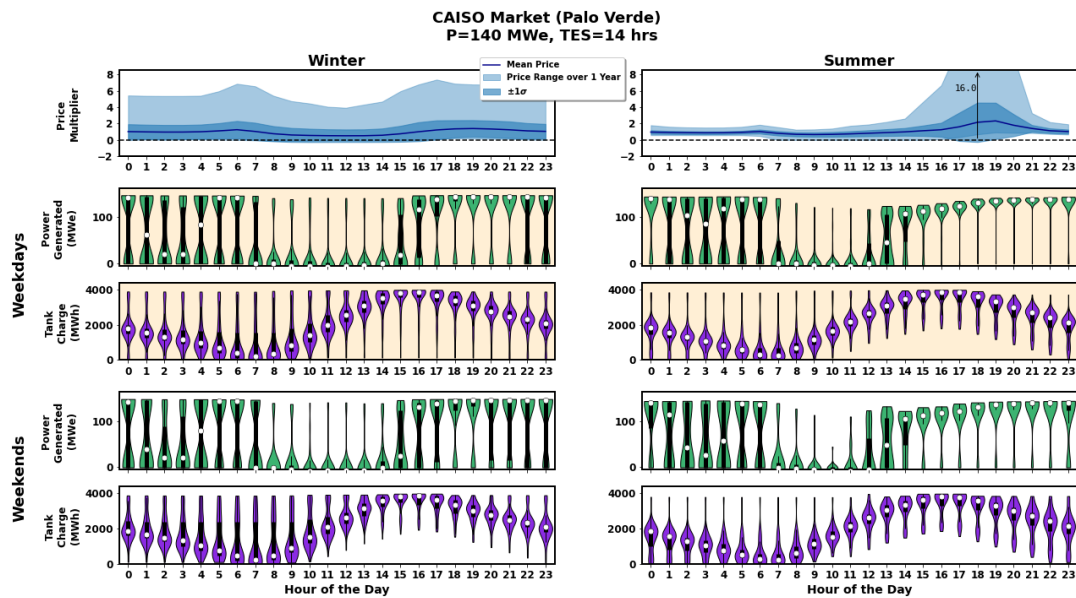


Figure 5: Hourly violin plot distributions for a year of electrical power production for an optimal CSP plant with CAISO tariff (Palo Verde)

The SAM generic tariff case has a relatively low storage capacity. The turbine tends to operate in the daytime and then switch off overnight. The small TES is used to maintain full power operation over the period where the solar irradiance drops, but prices remain higher. In contrast, both CAISO cases show the turbine generally switching off in the day while the TES charges, and then the plant operating through the late afternoon, evening, and night, slowly discharging the TES.

### 3.2. Nuclear Cases

A similar procedure is now used to optimize the reference nuclear-only cases (950 MWth nuclear plant), where the solar plant is omitted from the simulation entirely. Results are shown in Table 3. The SAM-generic and Iron Mountain 2019 cases largely replicate Ref. [16]. The SAM-generic tariff case likewise concludes that the best case is not to include a TES (and hence the nuclear plant operates at 100% all the time). However, the turbine cost curve has been changed and therefore the optimal configuration has a larger turbine than in the previous study. The same optimum is reached for the Palo Verde 2022 case.

Table 3: Optimized Nuclear Plant Configurations

Tariff	SAM Generic	Iron Mountain 2019	Palo Verde 2022
Turbine size (MWe)	450	900	900
TES Capacity (hr)	0	4	4
Year 1 PPA price (c/kWh)	6.46	5.51	6.06
Capacity Factor	100%	47%	47%

Violin plots for the CAISO cases are given in Figure 5 and Figure 6. In both cases, the TES is again charged in the day, and discharged in the evening. There is also some charging of the TES after midnight to service electrical loads in the morning.

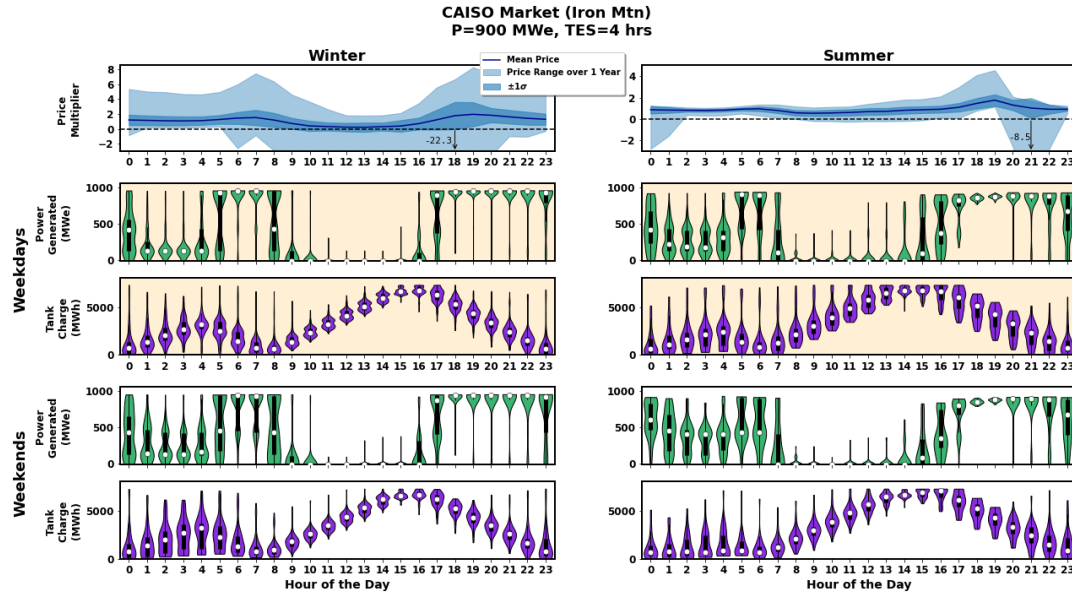


Figure 6: Hourly violin plot distributions for a year of electrical power production with an optimal nuclear plant, CAISO tariff (Iron Mountain)

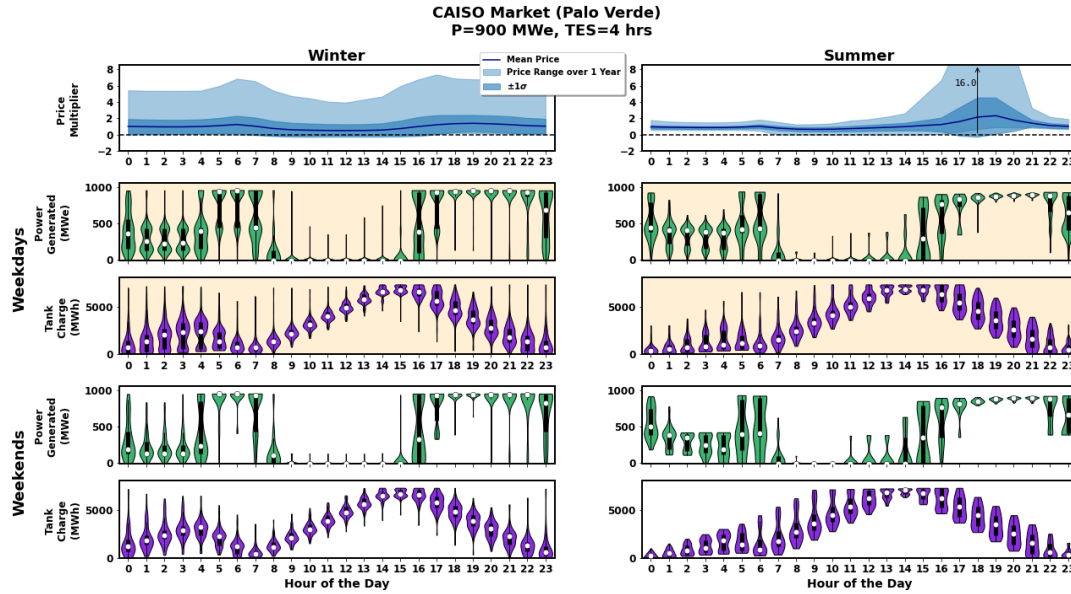


Figure 7: Hourly violin plot distributions for a year of electrical power production with an optimal nuclear plant, CAISO tariff (Palo Verde)

The behavior is very similar to that observed in Ref. [16]. Charging usually occurs both in the early hours of the morning and, most significantly, in the middle of the day. In both cases, this allows energy to be available for dispatch at the times of highest prices – most significantly in the evening, but also in the morning peak. The charging overnight varies somewhat to accommodate the morning demand, where higher prices are sustained for a lower period than in the evening.

Finally, the performance of the system when the nuclear reactor thermal output is varied is evaluated (Table 4). The ratio of the turbine capacity to the thermal output of the nuclear reactor is unchanged in each case. The TES capacity is also fixed in terms of hours of full-load storage. As a result, the dispatch behavior of the system stays the same. The system cost varies as a result of the turbine cost curve. Note that in reality, economies of scale would also apply to other components of the reactor. Here, these are neglected because the purpose of this study is to compare the performance of the hybrid system with separate solar and nuclear plants, which in principle leads to a slight economy of scale in the turbine sizing. For a given nuclear plant size, the change in the reactor capital cost with thermal output is neglected to simplify the comparison, although this assumption is revisited and justified in the next section.

Table 4. PPA price (c/kWh) as a function of nuclear reactor size

Nuclear Reactor Size (MWth)	SAM	Iron Mountain 2019	Palo Verde 2022
20	7.23	6.57	7.24
100	6.86	6.03	6.62
250	6.71	5.81	6.38
950	6.53	5.59	6.15
1900	6.46	5.51	6.06

### 3.3. Combined Cases

We now consider the case, where the nuclear and solar plants charge the same TES. The size of the solar power tower is kept fixed to 670 MWth, while the thermal output of the nuclear reactor is varied from 20 MWth to 1900 MWth as shown in Table 4, to determine if there is a synergy benefit in having both share the same TES, and whether this benefit varies with the relative size of each system. For each reactor thermal size, the TES capacity and turbine nominal capacity are the sum of those for the separate plants analyzed in Sections 3.1 and 3.2. This is discussed further below.

While the absolute cost of the system depends on size, the relative dispatch schedule for a given plant configuration is size-independent. Some minor variation in the optimal plant design is observed if the whole system is scaled up or down as a result of the nonlinearity in the turbine cost curve, which is not considered here.

It is anticipated that as the nuclear reactor becomes very large, any benefit from synergizing with the solar plant should become small, as the relative contribution of the power tower becomes less important. Similarly, as the nuclear reactor size decreases towards zero, the solar input should dominate the system. Therefore, any synergy benefit or otherwise would be most prominent at intermediate sizes.

The turbine size of the hybrid case is the sum of the turbine sizes  $P$  in the solar-only case and nuclear-only case. This is also the case for the TES capacity, noting that this is typically expressed in hours of inventory needed to provide full-load thermal input to the turbine. Hence the TES capacity of the hybrid case is:

$$TES_{hybrid}(hrs) = \frac{TES_{solar}(hrs) \times P_{solar}(MWe) + TES_{nuclear}(hrs) \times P_{nuclear}(MWe)}{P_{solar}(MWe) + P_{nuclear}(MWe)} \quad (5)$$

In each case, the performance of the hybrid case is compared to the combined output of separate solar and nuclear plants. That is, the summed results of a nuclear reactor of that size and the reference solar plant, with the PPA price calculated according to the total electricity output and cost of the combined system illustrated in Figure 8. Therefore, if the PPA price is lower for the hybrid case this indicates a synergy to sharing the TES and turbine, and vice versa. The modelled cases are therefore as in Table 5.

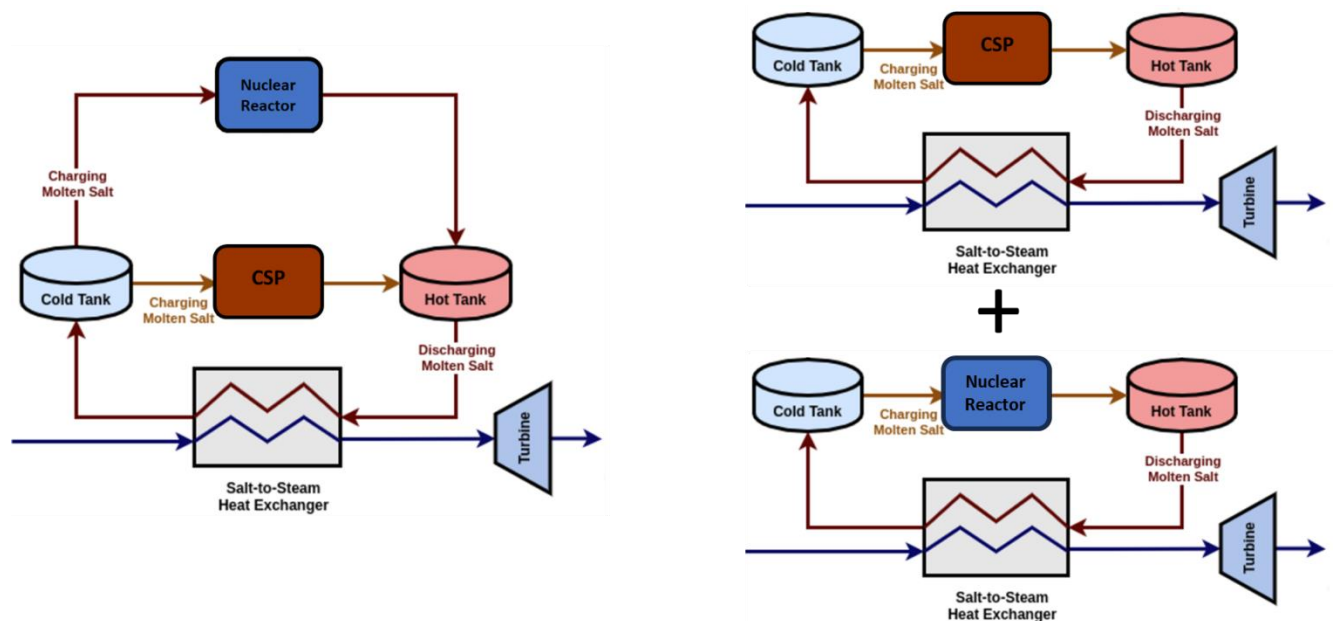


Figure 8: Structure of the hybrid cases. The hybrid case (left) contains equivalent components to separate cases (right). The nuclear reactor and CSP (left) are the same size as in the separate cases (right). The turbine and cold & hot tanks in the hybrid case (left) have capacities equal to the sum of the cases in the separate cases (right)

Table 5: Design results for the hybrid solar-nuclear cases. Note that in each case, the solar power tower is fixed while the turbine size and TES size are optimized.

Tariff	SAM		Iron Mountain 2019		Palo Verde 2022	
Nuclear Reactor Size (MWth)	Turbine Size (MWe)	TES Size (hrs)	Turbine Size (MWe)	TES Size (hrs)	Turbine Size (MWe)	TES Size (hrs)
20	270	0.96	159	14.6	159	12.8
100	307	0.85	235	11.2	235	9.97
250	378	0.69	377	8.46	377	7.15
950	710	0.37	1040	5.62	1040	5.35
1950	1160	0.22	1940	4.87	1940	4.72

A sensitivity analysis was also performed for the hybrid case, where the turbine size and TES capacity were varied around the values in Table 5, for the Iron Mountain 2019 tariff across different nuclear thermal output sizes. It was found that the PPA of the cases from Table 5 was within ~0.5% of the lowest achievable PPA at a given nuclear reactor size. This indicates that (1) deriving the size of the hybrid plant by summing the solar-only and nuclear-only cases is justified for the purposes of comparison (2) the assumption that the turbine size and TES capacity scale for the nuclear-only cases appears valid. In general, PPA variations for slight changes in turbine size and TES capacity around the design point tend to be small.

Results for PPA price are shown in Table 6. The percentage reduction in PPA from the hybrid plant compared to the separate plants is given in Figure 9.

Table 6: PPA price (c/kWh) for the hybrid plant compared to separate nuclear and solar plants, summed together. Hybrid plant has same volume of TES, overall turbine capacity and nuclear & CSP designs as the separate plants.

Tariff	SAM		Iron Mountain 2019		Palo Verde 2022	
Nuclear Reactor Size (MWth)	Separate Plants	Hybrid Plant	Separate Plants	Hybrid Plant	Separate Plants	Hybrid Plant
20	7.81	7.81	8.19	7.68	8.58	8.27
100	7.46	7.88	7.45	6.73	7.91	7.35
250	7.13	7.15	6.78	6.22	7.28	6.8
950	6.70	6.79	5.97	5.7	6.51	6.26
1950	6.56	6.57	5.72	5.57	6.26	6.12

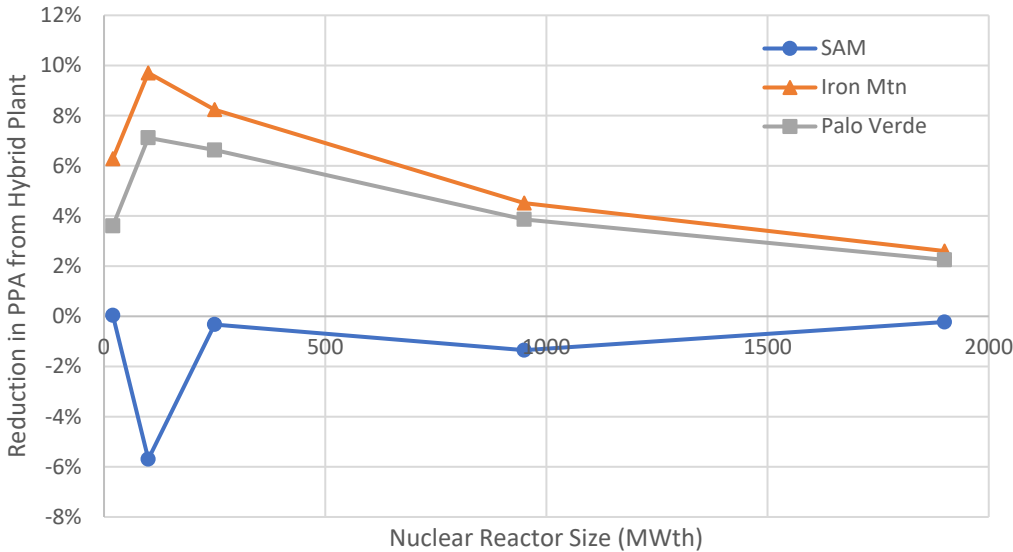


Figure 9: Reduction in PPA realized by hybrid plant in comparison to the combined output of two separately operating plants

For the CAISO tariffs, there is an appreciable synergy to combining the plants. This is larger when the nuclear thermal output is similar to that of the solar plant and drops off as anticipated as the nuclear plant becomes large or small relative to the solar plant. However, with the SAM tariff the combined plant exhibits a slight anti-synergy over most nuclear reactor sizes, and a strong anti-synergy when the solar and nuclear plants are of similar size – i.e., separate plants perform better than the combined plant.

To investigate the lattermost observation further, the PPA price of the hybrid plant is calculated for a few intermediate cases around 100 MWth (Figure 10). It is found that instead of monotonically falling with nuclear reactor size, the PPA slightly increases from 20 to 100 MWth, before falling again. This confirms the effect is reproducible over a range of similar powers. There is therefore a synergy from combining the plants when there is high price volatility, but an anti-synergy when there is low price volatility. The magnitude of this synergy/anti-synergy is greatest when the plants have similar contributions for thermal output. The reasons for this behavior are discussed further below.

We again note that the goal of this study is not to compare CSP and nuclear techno-economics – the difference in price between CSP-only and nuclear-only for the numbers used in this study should not be used to infer that it is uneconomic to use CSP relative to nuclear – in particular because the costs used for nuclear are estimated future cost and not actual cost.

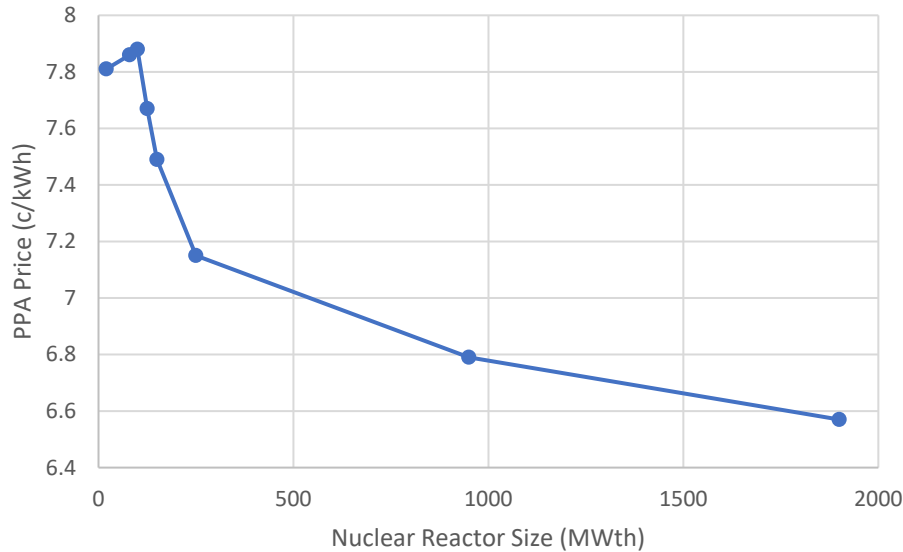


Figure 10: PPA price for a hybrid plant with SAM tariff as a function of nuclear reactor size (MWth) with greater simulation detail in the anti-synergy region where PPA price increases relative to the baseline separate plant case

The electrical output over the year for each case is now investigated with performance results summarized in Table 7. As the thermal output in each case is the same, variations in the electrical output are due to variations in turbine performance (and, to a lesser extent, thermal losses from the TES). With the SAM tariff, the electrical output is lower with the hybrid plant than for separate plants, whereas with the CAISO tariffs it is higher. This drives the difference in relative performance between the two cases.

Table 7. Total electricity produced for the three tariff cases at various nuclear reactor thermal capacities. Annual production is shown for the hybrid configuration and for the baseline separate-plant configuration.

Tariff	SAM		Iron Mountain 2019		Palo Verde 2022	
Nuclear Reactor Size (MWth)	Separate Plants (MWe yr)	Hybrid Plant (MWe yr)	Separate Plants (MWe yr)	Hybrid Plant (MWe yr)	Separate Plants (MWe yr)	Hybrid Plant (MWe yr)
20	74	72	74	78	77	78
100	112	101	109	116	112	115
250	183	176	175	183	179	183
950	519	509	485	494	489	495
1950	973	960	906	914	910	916

The percentage increase in total electrical output is now subtracted from the percentage decrease in PPA price and plotted in Figure 11. This isolates the change in annual electrical output due to hybridization from other potentially confounding effects of the hybrid plant such as cost reduction due to the turbine synergy and shared TES. The turbine synergy (i.e., the economy of scale effect from having one large turbine instead of two small ones) can be calculated to be of order 1%. Therefore, this isolates the benefit from sharing the TES to be at most approximately 3%.

This peak is observed when the nuclear reactor and solar power tower have similar electrical outputs and less when there is a size mismatch between them. That is, the location of the peak is at around 100-250 MWth nuclear reactor output, at which the nuclear plant contributes ~40-100 MWe on average, compared to ~65 MWe for the solar plant. The maximum dispatch synergy is a function of relative size, not absolute size. This makes intuitive sense, as if the nuclear plant is much larger than the solar plant, then the solar plant will not significantly influence the dispatch schedule, and vice versa.

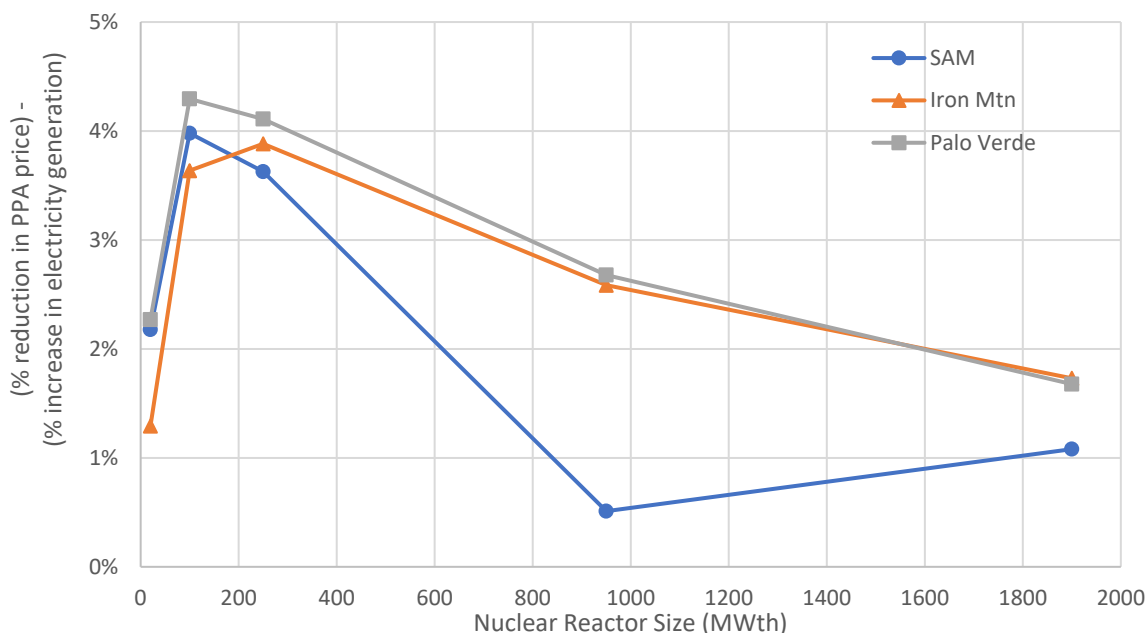


Figure 11: Difference between % reduction in PPA price and % increase in electricity generation.

The performance under different dispatch schedules is also used to examine the performance of the hybrid plant relative to separate plants. With the default tariff and a large (1900 MWth) nuclear reactor, the hybrid TES is small (0.2 hrs) and the turbine operates close to its design point all the time, using the TES to generate additional revenue in periods of higher prices (Figure 12). With a smaller nuclear reactor (100 MWth shown in Figure 13), the behavior is more similar to the solar only plant. However, there are periods where the turbine operates at low power in the late evening or morning. This turbine/ TES combination is not sufficiently large to discharge the full nuclear thermal output during the periods of high prices, and therefore must discharge nuclear at other times of day; however this underutilizes the turbine and therefore leads to inefficiencies in turbine operation, causing the anti-synergy that is observed. Nonetheless, as shown in Figure 11, the nuclear reactor is able to take advantage of the TES to better exploit changes in electricity prices than the separate plants. This appears to arise from fully charging the TES overnight using the nuclear reactor, which is the optimal time to charge it and is not otherwise available to the separate solar plant.

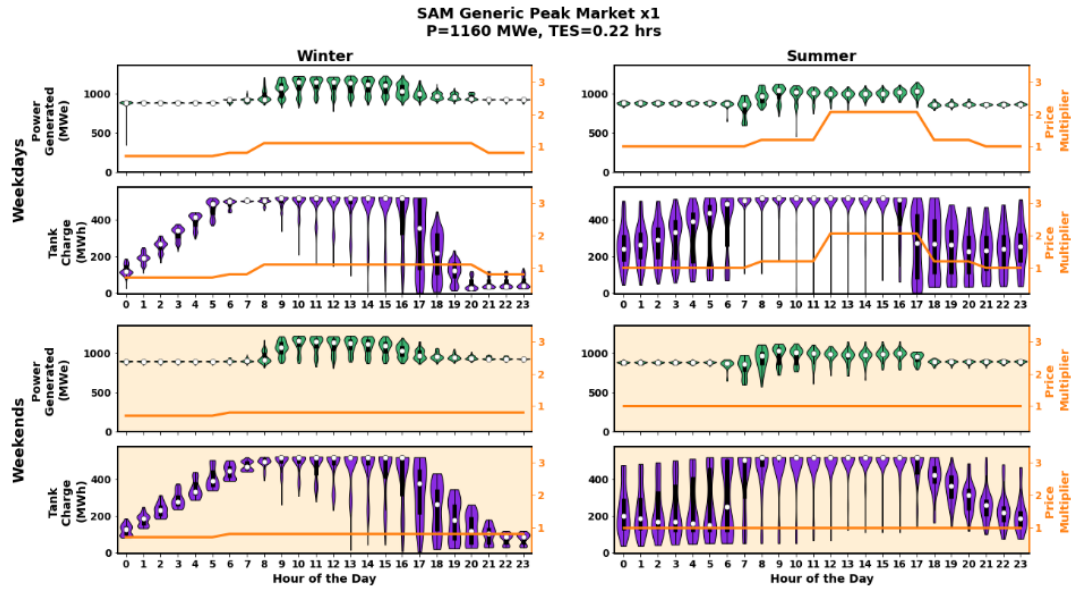


Figure 12: Hourly violin plot distributions for a year of electrical power production with hybrid 1900 MWth nuclear plant and CSP plant with SAM tariff

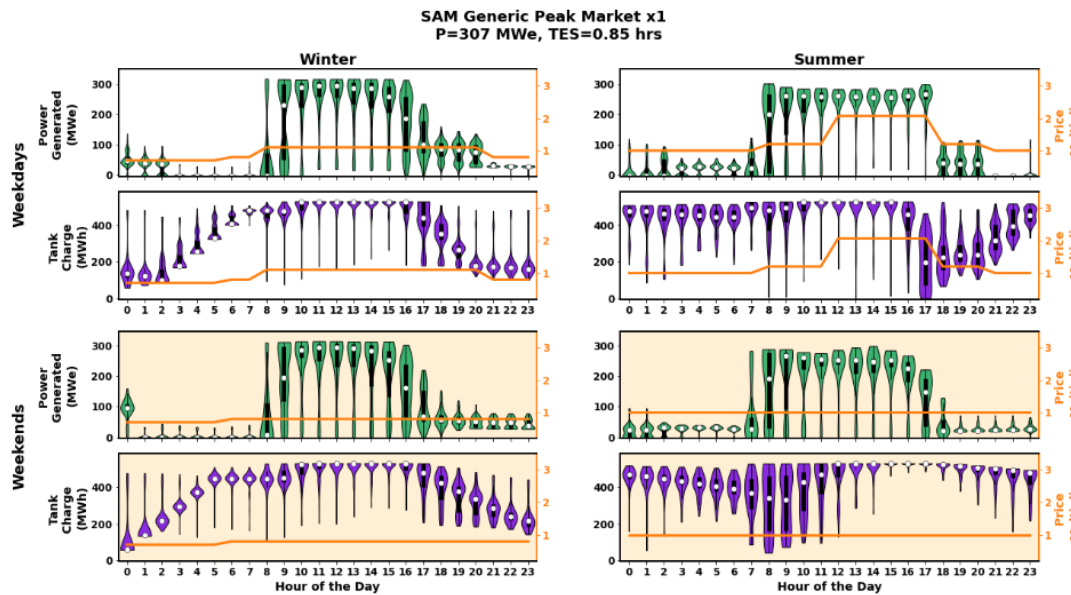


Figure 13: Hourly violin plot distributions for a year of electrical power production with hybrid 100 MWth nuclear plant and CSP plant with SAM tariff

The cause of the anti-synergy was also confirmed in a separate exercise, wherein the turbine performance was modified to achieve the same thermodynamic efficiency regardless of inlet conditions. In that case, the hybrid plant outperformed the separate plants by the same order as that predicted from Figure 11. While unphysical, this confirms the cause of the anti-synergy is the turbine performance.

In the CAISO market scenario, the dispatch behavior of the hybrid plant is similar to that of the separate plants in that both the nuclear and solar plants tend to produce power at the same times of day (afternoon, evening and morning) and shut down or produce low power around similar periods (after midnight and middle of the day). This is observed in both CAISO tariffs with 100 MWth and 250 MWth nuclear reactors and shown in Figure 14 – Figure 17. With similarly sized plants, the analysis indicates that synergy benefits of approximately 3% arise from both increased electrical output (i.e., better use of the turbine) and increased revenue (i.e., generating electricity at a more attractive time of day), for a 6% total synergy. It is difficult to isolate individual causes from the dispatch plots, but we offer a few observations:

- A reduction in low-power operation after midnight compared to the nuclear-only case could reduce turbine off-design performance, increasing electrical output. In Figure 14 – Figure 17 there is generally only one charge/discharge cycle per day (although discharge is slow or sometimes nearly flat in the early hours of the morning), whereas in the nuclear only cases, there was generally some charging behavior in the early hours of the morning.
- The nuclear reactor has access to the large thermal storage originally attributed to the solar case, while the solar output has access to a larger turbine to discharge the solar thermal energy collected in the middle of the day. This appears to improve the system’s ability to target the higher prices on winter mornings and avoid generating during lower price periods in the middle of the day.

Furthermore, the average thermal energy stored in the hybrid case is 5% lower than in the separate cases, leading to slightly lower thermal losses. However, the ultimate impact on electricity production is negligible.

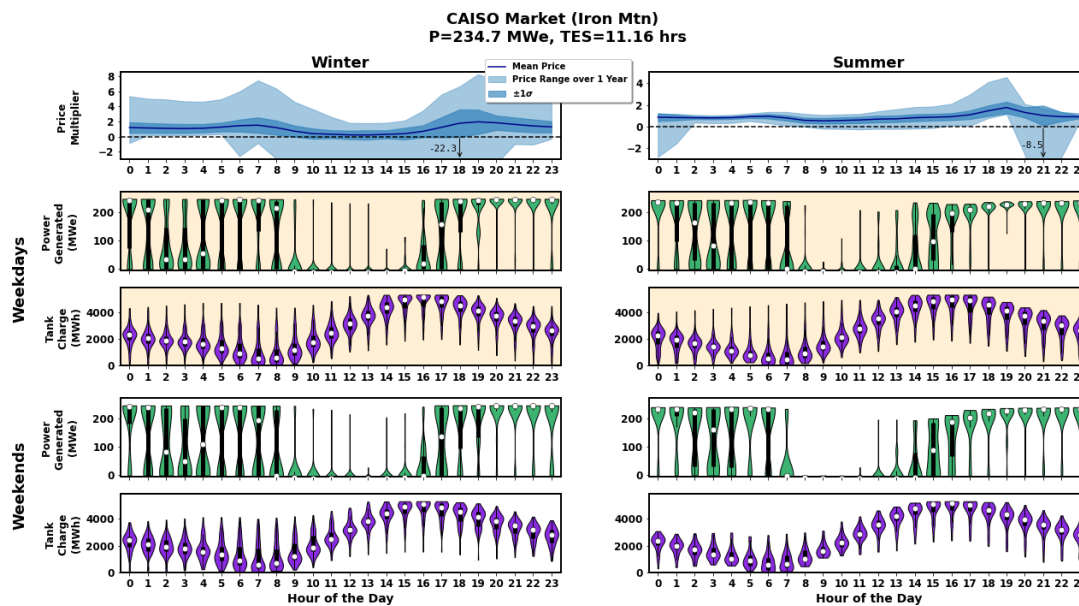


Figure 14: Hourly violin plot distributions for a year of electrical power production with hybrid 100 MWth nuclear plant and CSP plant with CAISO tariff (Iron Mountain)

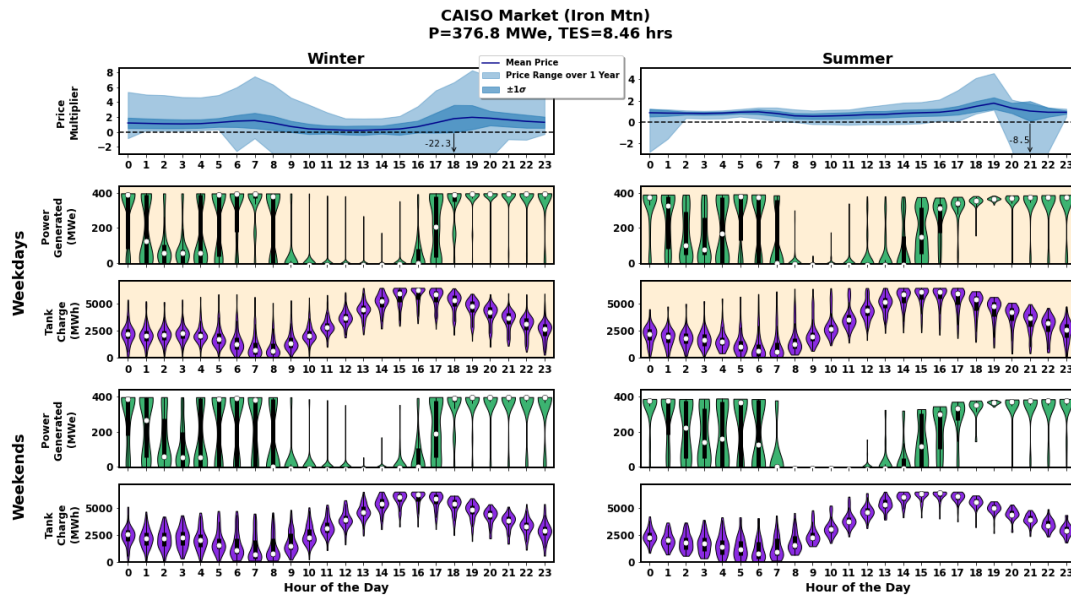


Figure 15: Hourly violin plot distributions for a year of electrical power production with hybrid 250 MWth nuclear plant and CSP plant with SAM tariff

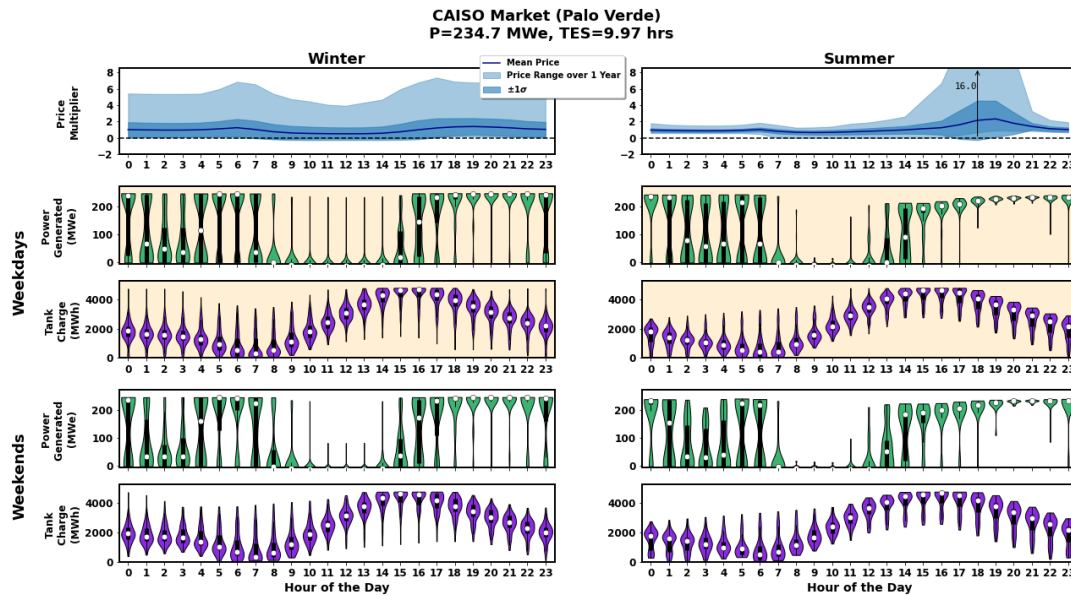


Figure 16: Hourly violin plot distributions for a year of electrical power production with hybrid 100 MWth nuclear plant and CSP plant with SAM tariff (Palo Verde)

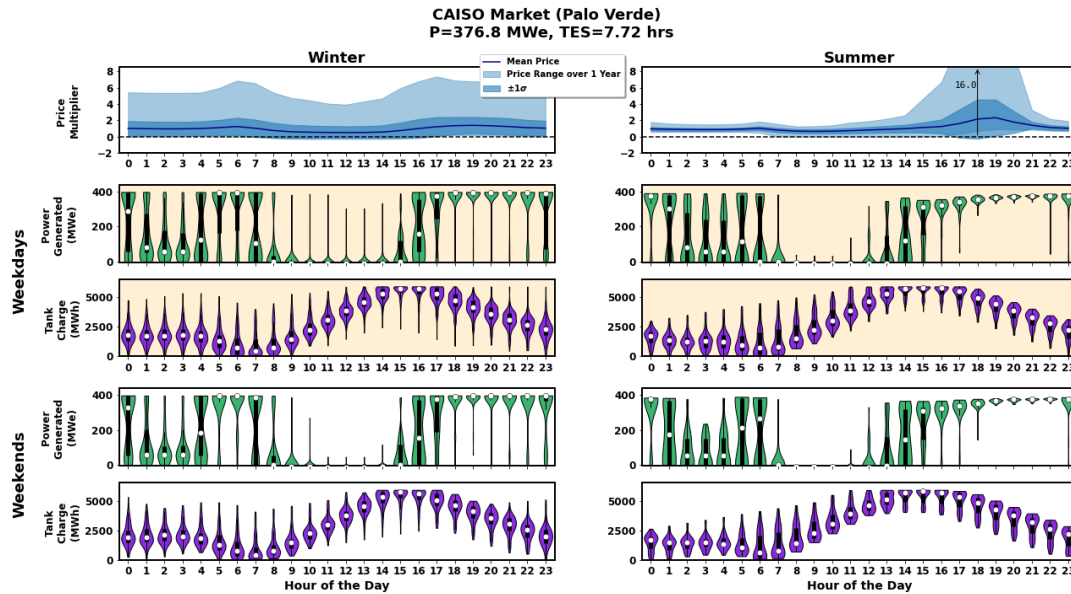


Figure 17: Hourly violin plot distributions for a year of electrical power production with hybrid 250 MWth nuclear plant and CSP plant with SAM tariff (Palo Verde)

#### 4. Conclusion

This study investigates the performance of a hybrid nuclear-solar thermal plant in which the nuclear reactor and concentrating solar power tower share molten salt TES. This arrangement gives rise to potential synergies in use of the shared TES and turbine. It is found that the benefit or otherwise of combining the TES in this manner depends upon the volatility of electricity prices. With relatively stable pricing, the nuclear reactor can operate nearly optimally without TES, effectively maintaining 100% output from the turbine as would occur in a separately located nuclear plant. When combining nuclear and solar as a hybrid plant, the turbine can be forced to operate away from its design point for a substantial fraction of the time, leading to inferior performance in comparison to separate plants.

Under the assumptions of this study, hybridized solar-nuclear plants operating subject to more volatile electricity prices (like those representative of CAISO) can result in a PPA price synergy benefit of up to 10%. This arises from three main drivers:

1. Improved ability of the hybrid plant to dispatch electricity at times of high electricity prices.
2. Improved ability of the hybrid plant to operate the turbine close to its design point, thereby improving electrical output.
3. Cost savings from economy of scale on the turbine.

The first benefit was maintained across two locations in CAISO with significant differences in prices. Additionally, this benefit was found in the case with low price volatility (although in that case it was negated by an anti-synergy from poor turbine performance). It can hence reasonably be concluded that the first benefit is general across locations.

The magnitude of the second benefit clearly depends on the details of the performance of the turbine, although the basic principle is expected to hold as turbine performance will in general drop away from the design point. It has also been shown to depend on the volatility of the electricity market. As the results for

the two CAISO cases were very similar, it can reasonably be assumed that the overall volatility of electricity prices is the key factor, rather than details of the day-to-day dispatch behavior. Given that volatile electricity prices are generally observed in areas of high solar penetration, it is likely that this benefit would be maintained if and where a hybrid plant were deployed. However, if the price volatility was less than that of CAISO but more than that of the generic tariff, it is anticipated that net benefit would fall somewhere in between. Hence, while the overall trends observed here are expected to be generally valid, it would be recommended to rerun the models with site- and turbine-specific data to reach a quantitative conclusion for a specific plant.

The third benefit is small (order of 1%) according to a typical power law turbine cost model and will also depend on the detailed plant design and available turbines (e.g., for very large plants there can be a diseconomy of scale if the turbine becomes customized). However, this is not the main factor driving the overall conclusions.

The impact of combining the plants is largest when the nuclear and solar thermal output is of the same order. Here, 100 MWth and 250 MWth nuclear reactors were combined with a solar plant at a 160 MWth design point to give the largest synergies. As the nuclear reactor became smaller or larger, the synergies reduced as the performance of one plant dominated over the other.

The potential benefit observed here must be balanced against costs associated with plant integration, including potential licensing and permitting hurdles, customization, and the need to co-site nuclear and solar thermal generators. With respect to the latter, plausible sites do exist in regions of high solar irradiance, for example Palo Verde as considered here.

## Acknowledgements

This work was supported by funding received from the DOE Office of Nuclear Energy's Nuclear Energy University Program under contract number DE-NE0008988. We express our thanks to Mr. Cory Stansbury of Westinghouse for his advice related to the engineering feasibility of IES coupling schemes and to Mr. Stefano Alarcon for his support on reviewing codes and standards for nuclear balance of plant.

## Appendix A

Linear constraints are applied within the MILP dispatch optimization problem to provide bounds on subsystem operations and ensure energy balance. Most constraints that are applied in the hybrid problem are detailed in in Refs. [16] and [20]. However, some constraints had to be updated to account for the dual-plant energy input. The first modified constraint is the grid sum constraint:

$$\begin{aligned} \dot{w}_t^s - \dot{w}_t^p = & (1 - \eta_t^c) \dot{w}_t - L^n (x_t^n + x_t^{nsu} + Q^{nl} y_t^{nsb}) - L^r (x_t^r + x_t^{rsu} + Q^{rl} y_t^{rsb}) - L^c x_t \quad (6) \\ & - W^h y_t^r - W^b y_t^{csb} - W^{ht} (y_t^{rsb} + y_t^{rsu}) - W^{nht} (y_t^{nsb} + y_t^{nsu}) \\ & - \frac{E^{hs}}{\Delta_t} (y_t^{rsu} + y_t^{rsb} + y_t^{rsd}) \end{aligned}$$

which subtracts losses from electric power produced. The constraint includes losses from both the nuclear plant, heliostat and receiver. Additional constraints are also updated for energy balance inside the thermal storage tanks:

$$s_t - s_{t-1} = \Delta_t [x_t^n + x_t^r - (Q_t^c y_t^{csu} + Q_t^b y_t^{csb} + x_t + Q^{nsb} y_t^{nsb} + Q^{rsb} y_t^{rsb})] \quad (7)$$

Which tracks the energy balance within the TES between time steps, allocating thermal power from both the nuclear reactor and CSP. It also allows extraction of energy for nominal PC operation, PC start-up and standby, nuclear and CSP stand-by. The final TES updated constraint is:

$$s_{t-1} \geq \Delta_t \delta_t^{ns} \left[ (Q^u + Q^b) (-3 + y_t^{rsu} + y_t^{nsu} + y_{t-1} + y_t + y_{t-1}^{csb} + y_t^{csb}) + x_t + Q^b y_t^{csb} \right] \quad (8)$$

Which ensures that the TES has sufficient capacity for start-up operations.

## References

- [1] A. D. Mills, T. Levin, R. Wiser, J. Seel, and A. Botterud, "Impacts of variable renewable energy on wholesale markets and generating assets in the United States: A review of expectations and evidence," *Renewable and Sustainable Energy Reviews*, vol. 120, p. 109670, Mar. 2020, doi: 10.1016/j.rser.2019.109670.
- [2] P. Denholm, M. O'Connell, G. Brinkman, and J. Jorgenson, "Overgeneration from Solar Energy in California. A Field Guide to the Duck Chart," National Renewable Energy Lab. (NREL), Golden, CO (United States), NREL/TP-6A20-65023, Nov. 2015. doi: 10.2172/1226167.
- [3] P. Denholm, J. C. King, C. F. Kutcher, and P. P. H. Wilson, "Decarbonizing the electric sector: Combining renewable and nuclear energy using thermal storage," *Energy Policy*, vol. 44, pp. 301–311, May 2012, doi: 10.1016/j.enpol.2012.01.055.
- [4] C. Forsberg, S. Brick, and G. Haratyk, "Coupling heat storage to nuclear reactors for variable electricity output with baseload reactor operation," *The Electricity Journal*, vol. 31, no. 3, pp. 23–31, Apr. 2018, doi: 10.1016/j.tej.2018.03.008.
- [5] "With Natrium, Nuclear Can Pair Perfectly with Energy Storage and Renewables," Nuclear Energy Institute. Accessed: Sep. 14, 2023. [Online]. Available: <https://www.nei.org/news/2020/natrium-nuclear-pairs-renewables-energy-storage>
- [6] E. González-Roubaud, D. Pérez-Osorio, and C. Prieto, "Review of commercial thermal energy storage in concentrated solar power plants: Steam vs. molten salts," *Renewable and Sustainable Energy Reviews*, vol. 80, pp. 133–148, Dec. 2017, doi: 10.1016/j.rser.2017.05.084.
- [7] A. m. Bayomy and M. a. Moore, "Nuclear renewable hybrid energy system assessment through the thermal storage system," *International Journal of Energy Research*, vol. 45, no. 8, pp. 11689–11711, 2021, doi: 10.1002/er.5514.
- [8] A. Naserbegi and M. Aghaie, "Exergy optimization of nuclear-solar dual proposed power plant based on GWO algorithm," *Progress in Nuclear Energy*, vol. 140, p. 103925, Oct. 2021, doi: 10.1016/j.pnucene.2021.103925.
- [9] D. Popov and A. Borissova, "Innovative configuration of a hybrid nuclear-parabolic trough solar power plant," *International Journal of Sustainable Energy*, vol. 37, no. 7, pp. 616–639, Aug. 2018, doi: 10.1080/14786451.2017.1333509.
- [10] B. Zhao, M. Cheng, C. Liu, and Z. Dai, "Conceptual design and preliminary performance analysis of a hybrid nuclear-solar power system with molten-salt packed-bed thermal energy storage for on-demand power supply," *Energy Conversion and Management*, vol. 166, pp. 174–186, Jun. 2018, doi: 10.1016/j.enconman.2018.04.015.
- [11] R. F. Benenati and J. R. Powell, "SOAR (Solar Assisted Reactor) power system," Brookhaven National Lab., Upton, NY (USA), BNL-25633; CONF-790602-29, Jan. 1979. Accessed: Sep. 14, 2023. [Online]. Available: <https://www.osti.gov/biblio/6322925>

- [12] A. C. G. Rigby, M. Wagner, and B. Lindley, "Dynamic Modelling of Flexible Dispatch in a Novel Nuclear-Solar Integrated Energy System with Thermal Energy Storage." Rochester, NY, Apr. 11, 2023. doi: 10.2139/ssrn.4528600.
- [13] S. Irish, "Terrestrial Energy IMSR Shows Value of Versatility," *Terrestrial Energy*. Accessed: Sep. 14, 2023. [Online]. Available: <https://www.terrestrialenergy.com/2022/09/terrestrial-energy-imsr-shows-power-of-versatility/>
- [14] T. W.- <https://www.techniquewebdesign.co.uk>, "GridReserve®: the future of energy storage," MoltexFLEX. Accessed: Sep. 14, 2023. [Online]. Available: <https://www.moltexflex.com/blog/gridreserve-the-future-of-energy-storage/>
- [15] J. M. Freeman *et al.*, "System Advisor Model (SAM) General Description (Version 2017.9.5)," National Renewable Energy Lab. (NREL), Golden, CO (United States), NREL/TP-6A20-70414, May 2018. doi: 10.2172/1440404.
- [16] G. J. Soto, B. Lindley, T. Neises, C. Stansbury, and M. J. Wagner, "Dispatch Optimization, System Design and Cost Benefit Analysis of a Nuclear Reactor with Molten Salt Thermal Storage," *Energies*, vol. 15, no. 10, Art. no. 10, Jan. 2022, doi: 10.3390/en15103599.
- [17] S. J. Lee, J. Liao, D. L. Wise, R. F. Wright, and P. Ferroni, "Preliminary assessment of the safety performance of Westinghouse LFR," *Nuclear Engineering and Design*, vol. 411, p. 112409, Sep. 2023, doi: 10.1016/j.nucengdes.2023.112409.
- [18] G. Brinkmann, "Modular HTR confinement/containment and the protection against aircraft crash," *Nuclear Engineering and Design*, vol. 236, no. 14, pp. 1612–1616, Aug. 2006, doi: 10.1016/j.nucengdes.2006.03.047.
- [19] F. Li, F. Chen, H. Wang, Y. Dong, and Z. Zhang, "One implementation of vented low pressure containment for HTR," *Nuclear Engineering and Design*, vol. 356, p. 110412, Jan. 2020, doi: 10.1016/j.nucengdes.2019.110412.
- [20] D. So and Y. B. Lee, "Security-by-Design Approach of the KALIMER-600 SFR Plant," in *Transactions of the Korean Nuclear Society Autumn Meeting*, Gyeongju, Korea, Oct. 2012. Accessed: Jun. 26, 2022. [Online]. Available: [https://www.kns.org/files/pre\\_paper/3/18%EC%86%8C%EB%8F%99%EC%84%AD.pdf](https://www.kns.org/files/pre_paper/3/18%EC%86%8C%EB%8F%99%EC%84%AD.pdf)
- [21] "Natrium," Natrium. Accessed: Feb. 18, 2024. [Online]. Available: <https://natriumpower.com/reactor-technology/>
- [22] M. J. Wagner and T. Wendelin, "SolarPILOT: A power tower solar field layout and characterization tool," *Solar Energy*, vol. 171, pp. 185–196, Sep. 2018, doi: 10.1016/j.solener.2018.06.063.
- [23] W. T. Hamilton, A. M. Newman, M. J. Wagner, and R. J. Braun, "Off-design performance of molten salt-driven Rankine cycles and its impact on the optimal dispatch of concentrating solar power systems," *Energy Conversion and Management*, vol. 220, p. 113025, Sep. 2020, doi: 10.1016/j.enconman.2020.113025.
- [24] ESMAP, "Study of equipment prices in the power section.," ESMAP Technical Paper 122/09, 2009. [Online]. Available: [https://www.esmap.org/sites/default/files/esmap-files/TR122-09\\_GBL\\_Study\\_of\\_Equipment\\_Prices\\_in\\_the\\_Power\\_Sector.pdf](https://www.esmap.org/sites/default/files/esmap-files/TR122-09_GBL_Study_of_Equipment_Prices_in_the_Power_Sector.pdf)
- [25] "OASIS - OASIS Prod - PUBLIC - 0." Accessed: Sep. 14, 2023. [Online]. Available: <http://oasis.caiso.com/mrioasis/logon.do>
- [26] K. Mayer and S. Trück, "Electricity markets around the world," *Journal of Commodity Markets*, vol. 9, pp. 77–100, Mar. 2018, doi: 10.1016/j.jcomm.2018.02.001.
- [27] M. J. Wagner, A. M. Newman, W. T. Hamilton, and R. J. Braun, "Optimized dispatch in a first-principles concentrating solar power production model," *Applied Energy*, vol. 203, pp. 959–971, Oct. 2017, doi: 10.1016/j.apenergy.2017.06.072.

- [28] J. L. Cox, W. T. Hamilton, A. M. Newman, M. J. Wagner, and A. J. Zolan, “Real-time dispatch optimization for concentrating solar power with thermal energy storage,” *Optim Eng*, vol. 24, no. 2, pp. 847–884, Jun. 2023, doi: 10.1007/s11081-022-09711-w.
- [29] M. L. Bynum *et al.*, *Pyomo — Optimization Modeling in Python*, vol. 67. in Springer Optimization and Its Applications, vol. 67. Cham: Springer International Publishing, 2021. doi: 10.1007/978-3-030-68928-5.
- [30] “Gurobi Optimizer Reference Manual,” Gurobi Optimization. Accessed: Sep. 14, 2023. [Online]. Available: <https://www.gurobi.com/documentation/current/refman/index.html>